Cross Sections for (α,n) Reactions for Medium-Weight Nuclei

P. H. STELSON AND F. K. MCGOWAN
Oak Ridge National Laboratory, Oak Ridge, Tennessee
(Received 20 September 1963)

Thick target (α,n) neutron yields have been measured from threshold to about 11-MeV α-particle energy for twenty targets ranging in A from 27 to 120. The targets of nickel, copper, and zinc were isotopically enriched. The absolute neutron yields, which were measured at approximately 100-keV energy intervals, have an accuracy of $\pm 4\%$. The neutron detector was the 4π, flat-energy response graphite sphere detector developed by Macklin. Cross sections for the (α,n) reactions were obtained to an accuracy of $\pm 15\%$ by differentiation of the smooth thick-target yield curves. For those nuclei in which the (α,n) cross section is thought to account for a significant percentage of the total reaction cross section, the observed cross sections are considerably larger than those predicted by Shapiro for his larger radial parameter of $1.5A^{1/3}$ F. Both the shape and absolute values of the observed cross sections agree fairly well with the optical-model analysis of reaction cross sections for α particles by Igo.

I. INTRODUCTION

THERE is surprisingly little experimental information on reaction cross sections for α particles on nuclei of intermediate weight for bombarding energies near to and below the potential barrier. In this energy region the predicted reaction cross section is quite sensitive to the assumed shape of the potential barrier. Shapiro[1] has calculated reaction cross sections for α particles by assuming a pure Coulomb barrier into a radius $(r_0A^{1/3}+1.21)$ F at which point the potential dropped sharply to a constant value of -5 MeV. He chose values for r_0 of 1.3 and 1.5 F. The reaction cross sections for Zn are shown in Fig. 1. The two assumed radii result in reaction cross sections which differ by a factor of 5 in the region well below the potential barrier.

It is now well known that the elastic scattering of α particles with energies considerably above the barrier (20 to 50 MeV) can be rather well fitted by optical-model analyses. The optical model also predicts the total reaction cross section. Igo[2] has used optical-model parameters obtained from elastic scattering (for example 40-MeV α particles on Cu) to predict reaction cross sections from 0 to 50 MeV on the assumption that these parameters are independent of α-particle energy.

The potential barrier which results from the combination of the nuclear optical potential and the Coulomb potential has a considerably different shape from that assumed in the early work of Shapiro. The barrier is both reduced and shifted to a larger radius. The natural consequence is that the predicted reaction cross sections are larger than those of Shapiro. Igo's predicted reaction cross section for Zn is also given in Fig. 1. For α-particle energies well below the barrier, the reaction cross section is 5 to 10 times larger still than those obtained by Shapiro with the larger of his two interaction radii.

Huizenga and Igo[3] have recently made additional calculations of α-particle reaction cross sections for different possible complex potentials. These results show that reaction cross sections are much more sensitive to variations in the complex potential parameters in the region below the classical barrier than in the region above the barrier.

From the above comments it is clear that the predicted reaction cross sections near to and below the barrier are quite sensitive to the parameters used to describe the nuclear potential. It likewise follows that predicted reaction cross sections, untested by experiment, are rather unreliable estimates. It was this fact which first interested us in this problem: we wanted to estimate the relative importance of Coulomb excitation and nuclear reaction cross sections in this energy region.

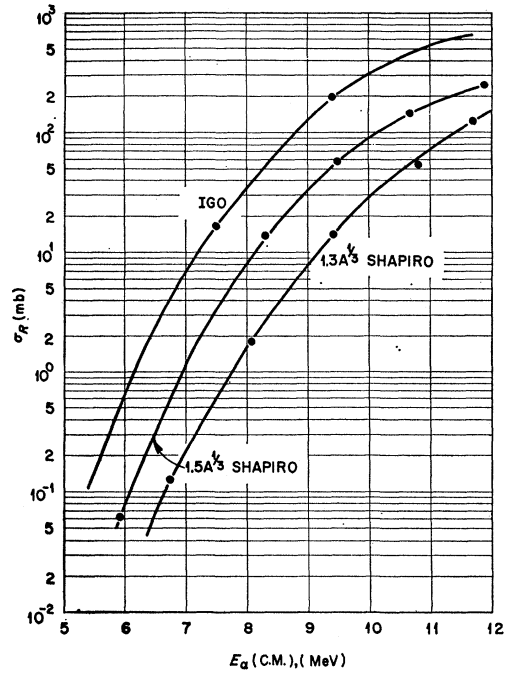

FIG. 1. Theoretical total reaction cross sections for zinc ($Z=30$). The two curves calculated by Shapiro are for the same model but with different radii. The curve calculated by Igo is based on an optical model obtained by fits to elastic scattering at higher α-particle energies.

[1] M. M. Shapiro, Phys. Rev. **90**, 171 (1953).
[2] G. Igo, Phys. Rev. **115**, 1665 (1959).
[3] J. R. Huizenga and G. Igo, Nucl. Phys. **29**, 462 (1962).

We have measured the absolute (α,n) cross sections for about twenty different targets ranging in A from 27 to 120. Cross sections were measured as a function of α-particle energy from the lowest feasible energy up to 11 MeV.

In general, for α-particle energies in this energy range (3 to 10 MeV), the possible reaction cross sections are (α,γ), (α,p), (α,n), and (α,α'). Since we have measured only the (α,n) cross section we have only a lower limit for the total reaction cross sections. However, it is expected that in many cases this limit will not be very different from the total reaction cross section and that it will therefore serve as a useful lower bound to possible theoretical estimates of the total reaction cross section.

Most of the (α,n) reactions in the mass region studied are endoergic reactions. When the Q value is sufficiently large (negative), the observed threshold is quite sharp. This allows the Q value to be measured with fair accuracy (± 40 keV). Eight Q values have been determined and these values are compared to the values based on the mass tables of Everling *et al.*[4]

II. EXPERIMENTAL METHOD

Variable energy α particles with energies up to 11.5 MeV were obtained by the acceleration of doubly ionized He in the ORNL 5.5-MV Van de Graaff. The output from the rf ion source contained a few tenths of 1% He^{++} ions. Both He^{+} and He^{++} were accelerated. The large He^{+} beam was caught on an air-cooled silver target mounted on the "mass 2" port of the analyzing magnet. The He^{++} beam was led through a 3-ft-thick water-wall shield to reduce the neutron background in the experimental area. The maximum beam current of He^{++} at the target was 0.25 μA.

Neutron yields from the (α,n) reactions were measured with the 5-ft-diam graphite sphere neutron detector developed by Macklin.[5] The high sensitivity, the flat energy response and the automatic averaging of the angular distribution make this an ideal instrument for this purpose. The efficiency variation with neutron energy is believed to be within $\pm 1\%$ for neutron energies from 1 keV to 2 MeV. At $E_n=5$ MeV the efficiency decreases by about 6% over that at lower energies.

The Q value for a typical (α,n) reaction is negative by several MeV. Therefore, in the energy range from threshold to $E\alpha=11$ MeV, the maximum neutron energy is typically 5 MeV and the efficiency variation is at most 6%. Actually, most of the emitted neutrons will have considerably less energy than the maximum and this ensures an even more constant efficiency.

The over-all efficiency of the graphite sphere detector is approximately 3%; the precise absolute value was determined to $\pm 4\%$ by calibration with a Ra-Be (γ,n) neutron source.

TABLE I. Representative stopping powers used to extract (α,n) cross sections. The stopping powers of other targets were obtained by making the assumption that the stopping power in (keV×cm²)/mg varies as $Z^{-1/2}$.

E_α(MeV)	$dE/d\rho x$[(keV×cm²)/mg] Al	Ni	Ag
5.0	586		
6.0	535	401	
7.0	496	366	
8.0	466	342	261
9.0	440	322	247
10.0	416	306	235
11.0	396	291	223

The graphite sphere detector automatically averages the angular distribution of the neutrons emitted by the target located at its center. It is estimated that an unidirectional beam of emitted neutrons would be detected with an efficiency which is only 1 to 2% different from an isotropic distribution.

Under favorable conditions, i.e., when the neutron yield of interest is large compared to other neutron yields, the error in the yield determination is primarily that caused by the uncertainty in the absolute calibration of the graphite sphere detector. Therefore, under favorable conditions the absolute neutron yields were measured to $\pm 4\%$.

To have an over-all check of the neutron yields measured by the graphite sphere, we also determined the neutron yield of the $Co^{59}(\alpha,n)Cu^{62}$ reaction by measuring the residual Cu^{62} activity.[6] The annihilation γ rays were detected in coincidence. It is estimated that the neutron yields from these measurements were determined to $\pm 6\%$. The comparison of the methods of measuring the $Co^{59}(\alpha,n)$ yields shows that in the α-particle energy range 7 to 10 MeV, the yields differed on the average by 1%.

In all cases, neutron yields were measured for thick metallic targets. Isotopically enriched targets of nickel, copper, zinc, and silver were prepared by electrodeposition. Electrodeposition was also used to prepare pure targets of normal cobalt and indium. The aluminum, molybdenum, zirconium, and palladium targets were commercial foils. In all cases the targets were sufficiently thick to completely stop 11-MeV α particles. The background counting rate was determined by bombarding a bright tungsten foil.

Cross sections were obtained by the differentiation of the measured thick target yield curves. This method has the virtue of not requiring the knowledge of the thickness of thin targets to determine cross sections. On the other hand, the method does require the knowledge of α-particle stopping powers. Representative

[4] F. Everling, L. A. Koenig, J. H. E. Mattauch, and A. H. Wapstra, Nucl. Phys. **15**, 342 (1960); **18**, 529 (1960).

[5] R. L. Macklin, J. Nucl. Instr. **1**, 335 (1957).

[6] F. K. McGowan, P. H. Stelson, and W. G. Smith, preceding paper, Phys. Rev. **133**, B907 (1964).

TABLE II. Summary of (α,n) neutron yields and cross sections for 18 targets. Columns 1 and 2 list, respectively, the target material and the incident α-particle energy in MeV. Column 3 lists the absolute neutron yield for one micro Coulomb of He^{++} particles (3.12×10^{12} incident partices) on a thick target. For targets made of isotopically enriched material, the yields have been corrected for possible contributions from other isotopes and have been increased to a 100% isotopic enrichment basis. Column 4 lists the derived (α,n) cross section in millibarns.

Target	E_α(MeV)	Yield Neutrons/μC	σ(mb)
Ni^{58}	10.8	1.27×10^{5}[a]	7.7
	10.9	2.25×10^{5}[a]	9.7
	11.0	3.40×10^{5}[a]	11.6
	11.1	4.75×10^{5}[b]	12.8
	11.2	6.25×10^{5}[b]	14.3
	11.3	7.97×10^{5}[b]	16.7
Ni^{60}	8.6	3.0×10^{4}[d]	1.65
	8.8	9.1×10^{4}[b]	8.7
	9.0	3.72×10^{5}	18
	9.2	8.17×10^{5}	27
	9.4	1.45×10^{6}	39
	9.6	2.37×10^{6}	50
	9.8	3.56×10^{6}	63
	10.0	5.03×10^{6}	77
	10.2	6.74×10^{6}	87
	10.4	8.78×10^{6}	106
	10.6	1.13×10^{7}	123
	10.8	1.41×10^{7}	139
Ni^{62}	7.2	4.2×10^{4}[a]	3.45
	7.4	1.37×10^{5}	6.5
	7.6	2.81×10^{5}	9.2
	7.8	4.86×10^{5}	13.8
	8.0	7.83×10^{5}	19.1
	8.2	1.19×10^{6}	24.5
	8.4	1.75×10^{6}	35
	8.6	2.56×10^{6}	49
	8.8	3.60×10^{6}	58
	9.0	4.88×10^{6}	67
	9.2	6.43×10^{6}	83
	9.4	8.34×10^{6}	106
	9.6	1.06×10^{7}	125
	9.8	1.35×10^{7}	146
	10.0	1.67×10^{7}	174
	10.2	2.07×10^{7}	193
	10.4	2.49×10^{7}	204
	10.6	2.97×10^{7}	243
	10.8	3.52×10^{7}	272
Co^{59}	5.8	6.2×10^{2}[c]	0.066
	6.0	2.7×10^{3}[b]	0.25
	6.2	8.1×10^{3}	0.45
	6.4	2.05×10^{4}	1.1
	6.6	4.45×10^{4}	1.8
	6.8	7.95×10^{4}	2.7
	7.0	1.44×10^{5}	4.7
	7.2	2.50×10^{5}	7.7
	7.4	4.12×10^{5}	11.2
	7.6	6.55×10^{5}	16.1
	7.8	9.87×10^{5}	20.7
	8.0	1.50×10^{6}	33.8
	8.2	2.22×10^{6}	44.3
	8.4	3.15×10^{6}	53.2
	8.6	4.38×10^{6}	75.7
	8.8	6.05×10^{6}	100
	9.0	8.16×10^{6}	120
	9.2	1.07×10^{7}	142
	9.4	1.38×10^{7}	171
	9.6	1.75×10^{7}	199
	9.8	2.17×10^{7}	216
	10.0	2.65×10^{7}	254
	10.2	3.21×10^{7}	300
	10.4	3.86×10^{7}	335
	10.6	4.60×10^{7}	350
	10.8	5.35×10^{7}	356
	11.0	6.14×10^{7}	363
Cu^{63}	8.4	5.9×10^{4}	5.3
	8.6	2.06×10^{5}	12.6
	8.8	5.10×10^{5}	20.5
	9.0	9.83×10^{5}	30.
	9.2	1.68×10^{6}	42
	9.4	2.56×10^{6}	53
	9.6	3.75×10^{6}	70
	9.8	5.25×10^{6}	82
	10.0	7.07×10^{6}	102
	10.2	9.21×10^{6}	121
	10.4	1.18×10^{7}	139
	10.6	1.48×10^{7}	154
Cu^{65}	6.4	1.36×10^{3}[a]	0.11 ± 0.02
	6.6	4.75×10^{3}[b]	0.36 ± 0.04
	6.8	1.52×10^{4}	0.90
	7.0	3.75×10^{4}	1.7
	7.2	7.36×10^{4}	2.9
	7.4	1.33×10^{5}	4.4
	7.6	2.31×10^{5}	6.7
	7.8	3.70×10^{5}	9.7
	8.0	5.91×10^{5}	14.7
	8.2	9.07×10^{5}	21
	8.4	1.34×10^{6}	29
	8.6	1.96×10^{6}	40
	8.8	2.77×10^{6}	48
	9.0	3.77×10^{6}	62
	9.2	5.12×10^{6}	80
	9.4	6.79×10^{6}	101
	9.6	8.83×10^{6}	119
	9.8	1.14×10^{7}	141
	10.0	1.43×10^{7}	158
	10.2	1.78×10^{7}	193
	10.4	2.18×10^{7}	218
	10.6	2.66×10^{7}	242
Zn^{66}	7.8	6.1×10^{3}[c]	
	8.0	2.76×10^{4}[b]	1.8
	8.2	7.46×10^{4}	3.5
	8.4	1.89×10^{5}	10.7
	8.6	4.47×10^{5}	18.3
	8.8	8.40×10^{5}	25
	9.0	1.40×10^{6}	35
	9.2	2.19×10^{6}	45
	9.4	3.14×10^{6}	58
	9.6	4.40×10^{6}	73
	9.8	5.91×10^{6}	89
	10.0	7.67×10^{6}	114
	10.2	1.03×10^{7}	130
	10.4	1.32×10^{7}	153
	10.6	1.63×10^{7}	173
	10.8	2.02×10^{7}	213
	11.0	2.47×10^{7}	231
Zn^{64}	9.8	2.68×10^{4}[a]	3.6
	10.0	1.45×10^{5}[b]	10.7
	10.2	4.69×10^{5}	23
	10.4	9.71×10^{5}	28
	10.6	1.62×10^{6}	39
	10.8	2.48×10^{6}	46
	11.0	3.55×10^{6}	59
	11.2	4.80×10^{6}	
Zn^{68}	6.4	2.06×10^{3}[a]	0.16 ± 0.04
	6.6	6.20×10^{3}[a]	0.36 ± 0.07
	6.8	1.41×10^{4}[b]	0.68 ± 0.05
	7.0	2.87×10^{4}	1.13 ± 0.08
	7.2	5.34×10^{4}	1.9

[a] $\pm10\%$. [b] $\pm5\%$. [c] $\pm15\%$. [d] $\pm20\%$.

TABLE II (*continued*).

Target	E_α(MeV)	Yield Neutrons/μC	σ(mb)
Zn^{68}	7.4	9.50×10^4	3.4
	7.6	1.62×10^5	4.9
	7.8	2.66×10^5	7.3
	8.0	4.14×10^5	9.8
	8.2	6.23×10^5	15
	8.4	9.37×10^5	20
	8.6	1.37×10^6	30
	8.8	1.99×10^6	37
	9.0	2.81×10^6	47
	9.2	3.77×10^6	65
	9.4	5.20×10^6	83
	9.6	6.94×10^6	98
	9.8	9.06×10^6	120
	10.0	1.16×10^7	139
	10.2	1.46×10^7	163
	10.4	1.80×10^7	197
	10.6	2.22×10^7	217
	10.8	2.69×10^7	248
Zn^{70}	6.2	1.37×10^4[d]	0.27±0.07
	6.4	1.85×10^4[c]	0.37±0.10
	6.6	2.65×10^4[a]	0.64±0.12
	6.8	4.01×10^4[b]	1.11±0.17
	7.0	6.24×10^4	1.61±0.19
	7.2	9.61×10^4	2.6
	7.4	1.48×10^5	3.6
	7.6	2.28×10^5	6.3
	7.8	3.52×10^5	9.8
	8.0	5.55×10^5	13.1
	8.2	8.04×10^5	17.2
	8.4	1.18×10^6	23
	8.6	1.72×10^6	36
	8.8	2.46×10^6	44
	9.0	3.33×10^6	53
	9.2	4.52×10^6	74
	9.4	6.07×10^6	89
	9.6	7.88×10^6	101
	9.8	1.01×10^7	128
	10.0	1.29×10^7	152
	10.2	1.60×10^7	159
	10.4	1.92×10^7	191
	10.6	2.34×10^7	216
	10.8	2.80×10^7	224
Al	5.2	1.33×10^6	20
	5.4	1.92×10^6	26
	5.6	2.67×10^6	32
	5.8	3.57×10^6	39
	6.0	4.67×10^6	50
	6.2	6.14×10^6	62
	6.4	8.00×10^6	74
	6.6	1.02×10^7	85
	6.8	1.26×10^7	103
	7.0	1.52×10^7	116
	7.2	1.86×10^7	124
	7.4	2.22×10^7	133
	7.6	2.60×10^7	135
	7.8	2.98×10^7	140
	8.0	3.42×10^7	152
	8.2	3.91×10^7	167
	8.4	4.43×10^7	175
	8.6	4.95×10^7	180
	8.8	5.52×10^7	200
	9.0	6.12×10^7	215
	9.2	6.77×10^7	230
	9.4	7.43×10^7	290
	9.6	8.13×10^7	350
	9.8	8.88×10^7	350
	10.0	9.63×10^7	350
	10.2	10.3×10^8	330
	10.4	1.14×10^8	310

Target	E_α(MeV)	Yield Neutrons/μC	σ(mb)
Al	10.6	1.26×10^8	295
	10.8	1.36×10^8	290
	11.0	1.46×10^8	290
Zr	8.8	$(2.5\ \pm1.0)\times10^4$	0.63±0.10
	9.0	$(3.6\ \pm1.0)\times10^4$	0.90±0.10
	9.2	$(5.5\ \pm1.0)\times10^4$	1.30±0.07
	9.4	$(8.0\ \pm1.0)\times10^4$	1.83
	9.6	$(1.15\pm0.10)\times10^5$	2.61
	9.8	$(1.70\pm0.15)\times10^5$	4.30
	10.0	$(2.4\ \pm0.2)\times10^5$	5.92
	10.2	$(3.7\ \pm0.3)\times10^5$	8.52
	10.4	$(5.4\ \pm0.4)\times10^5$	12.4
	10.6	$(7.8\ \pm0.5)\times10^5$	17.4
	10.8	$(1.11\pm0.05)\times10^5$	22.5
	11.0	$(1.57\pm0.06)\times10^5$	31
Nb^{93}	8.6	$(1.28_{-0.5}^{+1.0})\times10^4$	0.32±0.08
	8.8	$(1.86_{-0.5}^{+1.0})\times10^4$	0.46±0.11
	9.0	$(2.73_{-0.6}^{+1.2})\times10^4$	0.65±0.13
	9.2	$(3.97_{-0.7}^{+1.5})\times10^4$	0.97±0.20
	9.4	$(5.72_{-1.0}^{+2.0})\times10^4$	1.32±0.26
	9.6	$(8.14_{-1.0}^{+2.0})\times10^4$	1.80±0.27
	9.8	$(1.19\pm0.20)\times10^5$	3.25±0.43
	10.0	$(1.76\pm0.20)\times10^5$	3.84±0.55
	10.2	$(2.63\pm0.25)\times10^5$	6.26±0.95
	10.4	$(3.86\pm0.35)\times10^5$	9.00±1.35
	10.6	$(5.63\pm0.40)\times10^5$	12.3 ±1.8
	10.8	$(8.05\pm0.40)\times10^5$	16.7 ±2.5
	11.0	$(1.14\pm0.05)\times10^6$	23.6 ±3.6
Mo	8.8	$(3.9\ \pm2.0)\times10^3$	0.15±0.04
	9.0	$(6.9\ \pm3.0)\times10^3$	0.26±0.06
	9.2	$(1.20\pm0.40)\times10^4$	0.44±0.09
	9.4	$(2.07\pm0.50)\times10^4$	0.72±0.14
	9.6	$(3.5\ \pm0.50)\times10^4$	1.18±0.17
	9.8	$(5.9\ \pm0.60)\times10^4$	1.88±0.27
	10.0	$(9.5\ \pm1.0)\times10^4$	2.72±0.40
	10.2	$(1.50\pm0.14)\times10^5$	4.26±0.63
	10.4	$(2.32\pm0.15)\times10^5$	6.20±0.93
	10.6	$(3.55\pm0.25)\times10^5$	9.09±1.35
	10.8	$(5.31\pm0.30)\times10^5$	12.9 ±1.8
	11.0	$(7.82\pm0.30)\times10^5$	18.3 ±2.7
Pd	9.8	$(7.5\ \pm3.7)\times10^3$	0.26±0.06
	10.0	$(1.26\pm0.50)\times10^4$	0.47±0.10
	10.2	$(2.19\pm0.50)\times10^4$	0.80±0.16
	10.4	$(3.74\pm0.50)\times10^4$	1.32±0.26
	10.6	$(6.25\pm0.50)\times10^4$	2.01±0.30
	10.8	$(9.93\pm0.60)\times10^4$	2.78±0.40
	11.0	$(1.50\pm0.08)\times10^5$	3.71±0.52
Ag^{109}	10.2	$(1.0\ \pm0.5)\times10^4$	0.38±0.16
	10.3	$(1.34\pm0.6)\times10^4$	0.50±0.15
	10.4	$(1.79\pm0.6)\times10^4$	0.68±0.17
	10.5	$(2.38+0.8)\times10^4$	0.86±0.21
	10.6	$(3.12\pm0.6)\times10^4$	1.08±0.22
	10.7	$(4.05\pm0.6)\times10^4$	1.34±0.27
	10.8	$(5.20\pm0.6)\times10^4$	1.63±0.33
	10.9	$(6.6\ \pm0.7)\times10^4$	1.96±0.40
	11.0	$(8.3\ \pm0.7)\times10^4$	2.30±0.46
Ag^{107}	10.2	$(6.1\ \pm3.0)\times10^3$	0.28±0.12
	10.3	$(8.5\ \pm4.0)\times10^3$	0.38±0.11
	10.4	$(1.2\ \pm0.5)\times10^4$	0.54±0.13
	10.5	$(1.7\ \pm0.6)\times10^4$	0.71±0.18
	10.6	$(2.3\ \pm0.6)\times10^4$	0.93±0.19
	10.7	$(3.1\ \pm0.6)\times10^4$	1.14±0.23
	10.8	$(4.1\ \pm0.6)\times10^4$	1.45±0.29
	10.9	$(5.35\pm0.7)\times10^4$	1.75±0.35
	11.0	$(6.85\pm0.7)\times10^4$	2.11±0.41

[a] ±10%. [b] ±5%. [c] ±15%. [d] ±20%.

TABLE II (*continued*).

Target	E_α(MeV)	Yield Neutrons/μC	σ(mb)
In	10.5	(1.0 ±0.5) ×10[3]	
	10.6	(2.7 ±1.0) ×10[3]	
	10.7	(5.6 ±2.0) ×10[3]	0.51±0.25
	10.8	(1.0 ±0.4) ×10[4]	0.70±0.21
	10.9	(1.6 ±0.5) ×10[4]	0.88±0.18
	11.0	(2.3 ±0.7) ×10[4]	0.99±0.20

[a] ±10%. [b] ±5%. [c] ±15%. [d] ±20%.

values for the stopping powers which we have used for aluminum, nickel, and silver are given in Table I. These values are in agreement with those obtained by Rosenblum.[7] It is estimated that the stopping powers are known to be ±8%.

In addition to the errors in efficiency calibration of the graphite sphere (±4%) and errors in the α-particle

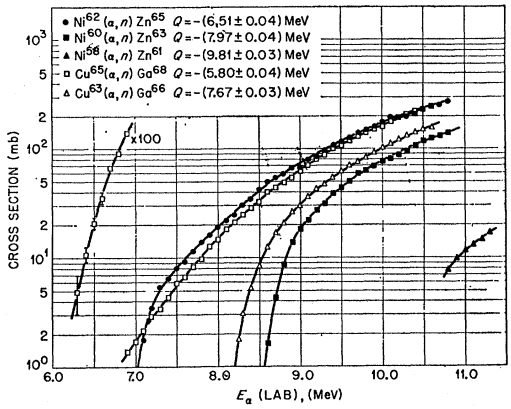

FIG. 2. Graphical summary of the measured (α,n) cross sections for the different isotopes of nickel and copper. Cross sections are given in millibarns.

stopping powers (±8%), both of which enter directly as errors in the absolute cross sections, there is also an error introduced by the differentiation of the yield curve. We estimate that this error is ±10%. Therefore, under favorable conditions, the absolute cross sections are determined to approximately ±15%.

III. RESULTS AND DISCUSSION

The values obtained for the thick target (α,n) yields for 18 different targets are listed in Table II. As previously mentioned, the yields are generally determined to ±4%. However, yields measured near to the threshold and yields measured for the higher Z targets have an additional error listed which should be combined with 4% to obtain to the total error. The observed yields varied from 10^3 to 10^8 neutrons/μC of He^{++}.

[7] S. Rosenblum, Ann. Phys. (Paris) **10**, 408 (1928); W. Whaling, *Handbuch der Physik*, edited by S. Flügge (Springer-Verlag, Berlin, 1958), Vol. 34, p. 193.

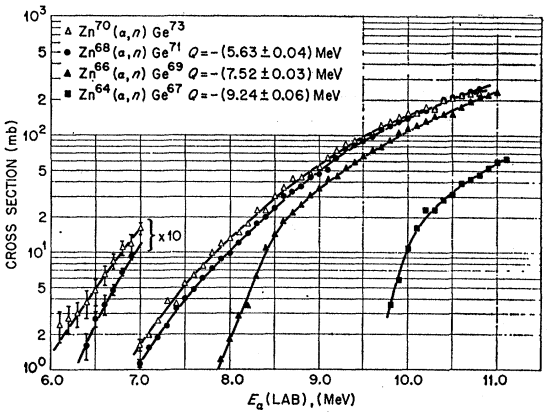

FIG. 3. Graphical summary of the measured (α,n) cross sections for the different isotopes of zinc.

The derived cross sections for the different target materials are also given in Table II. The values vary from ~0.1 mb to several hundred millibarns. The cross sections have an estimated error of ±15%. When an error is listed with the cross section, this error should be combined with a 15% error to obtain the estimated total error.

The cross sections for the separated isotopes of

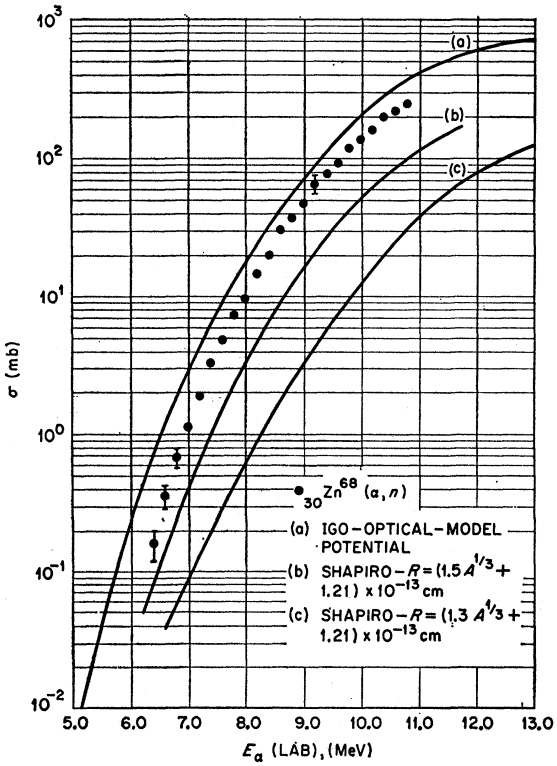

FIG. 4. Comparison of the observed $Zn^{68}(\alpha,n)$ cross section with the total reaction cross sections calculated by Shapiro and Igo. The Shapiro values are clearly too small. The (α,n) cross sections are consistent with Igo's prediction. The (α,p) contribution to the total reaction cross section is not known.

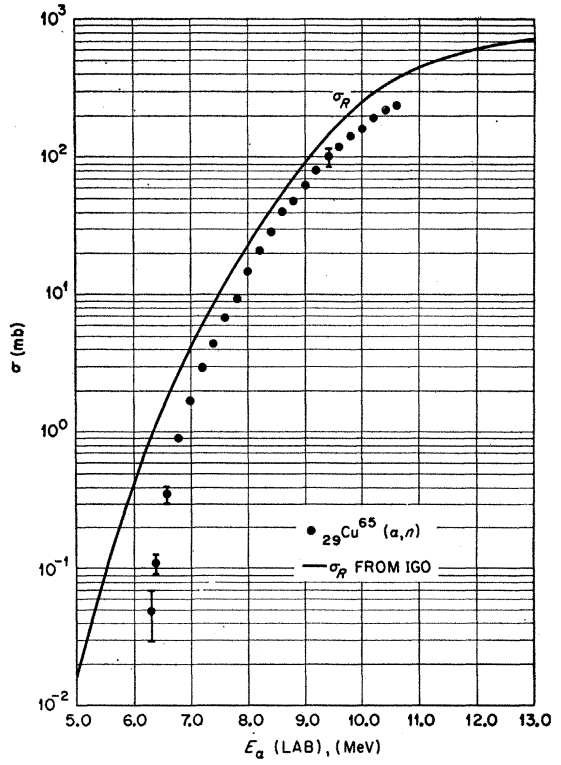

FIG. 5. Comparison of the $Cu^{65}(\alpha,n)$ cross section with the total reaction cross section predicted by Igo. The (α,p) contribution to the total reaction cross section is not known.

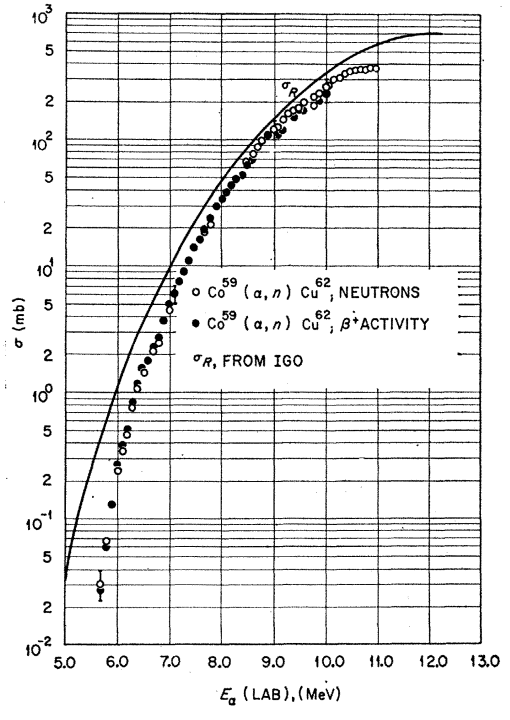

FIG. 6. Comparison of the $Co^{59}(\alpha,n)$ cross section with the total reaction cross section calculated by Igo. The (α,n) cross section was determined both by measuring the neutron yield and by measuring the induced position activity.

copper, nickel, and zinc are shown in Figs. 2 and 3. Some understanding of the variation in the behavior of these (α,n) cross sections for the different isotopes is obtained by considering the variation of the Q values for (α,n) and (α,p) reactions for nuclei in this region. The Q values for both types of reactions are generally negative, so that thresholds exist. However, the thresholds for (α,n) reactions vary appreciably and systematically from isotope to isotope. The heavier the isotope, the lower the threshold. For example, the thresholds for (α,n) reactions on Zn^{64}, Zn^{66}, Zn^{68}, and Zn^{70} are, respectively 9.8, 8.0, 6.2, and 4.0 MeV. On the other hand, the (α,p) thresholds are in general lower than the (α,n) thresholds and are relatively constant for different isotopes. For Zn^{64}, Zn^{66}, Zn^{68}, and Zn^{70}, the

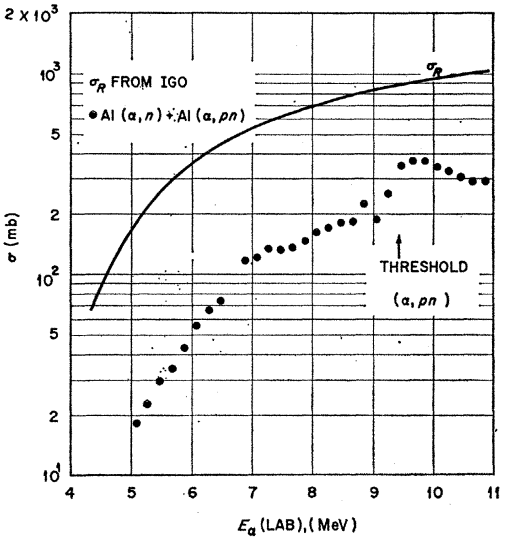

FIG. 7. The $Al(\alpha,n)$ cross section is compared to Igo's predicted total reaction cross section. At higher energies the (α,pn) reaction is also energetically possible.

(α,p) thresholds are, respectively, 4.2, 4.5, 5.1, and 4.8 MeV.

At 1 MeV above the (α,n) threshold for Zn^{64}, the (α,n) cross section is still 6 times less than the (α,n) cross section for Zn^{70} at that energy. The (α,p) threshold for Zn^{64} is only 4.2 MeV. Apparently, the additional available energy and the many more available states for proton decay don't allow neutron emission to compete very favorably with proton emission for Zn^{64}. On the other hand, for Zn^{70} both (α,p) and (α,n) thresholds are low and in this case the (α,n) cross section is very likely comparable or somewhat larger than the (α,p) cross section.

Similar systematic cross section variations for isotopes of copper and nickel can be understood in terms of the above argument for Zn^{64} and Zn^{70}. An extreme case is Ni^{58} where the (α,n) cross section is a factor of 25 less than that for Ni^{62} at $E_\alpha=11$ MeV. From this

result one infers that the (α,p) reaction on Ni^{58} at 11 MeV is about 25 times more likely than the (α,n) reaction. For this particular nucleus, the (α,p) cross section has been measured and found to be 25 times larger than the (α,n) cross section.[6]

Therefore, from the observed behavior of the (α,n) cross sections it follows that the (α,n) cross sections for the heavier isotopes of each element should be a reasonably close approximation to the total reaction cross section whereas those for the lightest isotope are only a small fraction of the reaction cross section. In Fig. 4 we have compared the observed (α,n) cross section for Zn^{68} with the predicted cross sections of

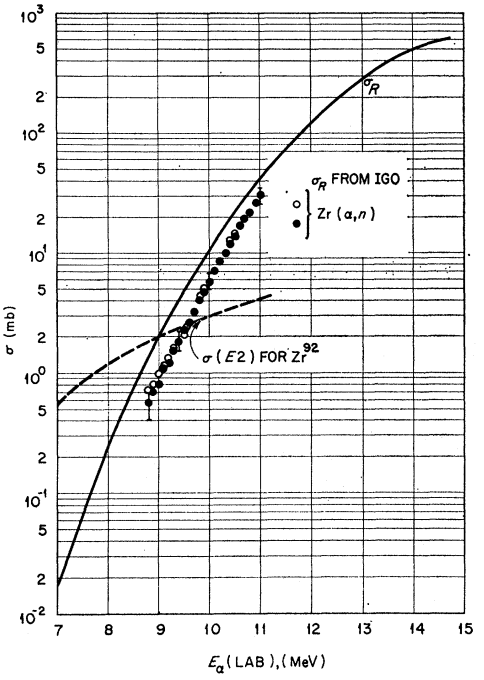

FIG. 8. The (α,n) cross section for normal zirconium is shown together with Igo's predicted total reaction cross section. The Coulomb excitation cross section for excitation of the first 2+ state in Zr^{92} is also shown.

Shapiro and Igo. It is clear that the reaction cross sections of Shapiro are too small. On the other hand, the shape and magnitude of Igo's predicted cross section agrees quite well, especially when allowance is made for a contribution from the unknown (α,p) cross section. Figures 5 and 6 show similar satisfactory agreement with Igo's predicted cross sections for Cu^{65} and Co^{59}.

The lightest nucleus studied was Al^{27}. The (α,n) cross section for Al^{27} is shown in Fig. 7. The (α,n) threshold for Al^{27} is 3.0 MeV whereas the (α,p) reaction actually has a positive Q value of about 2 MeV. The observed (α,n) cross section is only a fraction of Igo's predicted reaction cross section. One must conclude that if the predicted cross section is correct then the

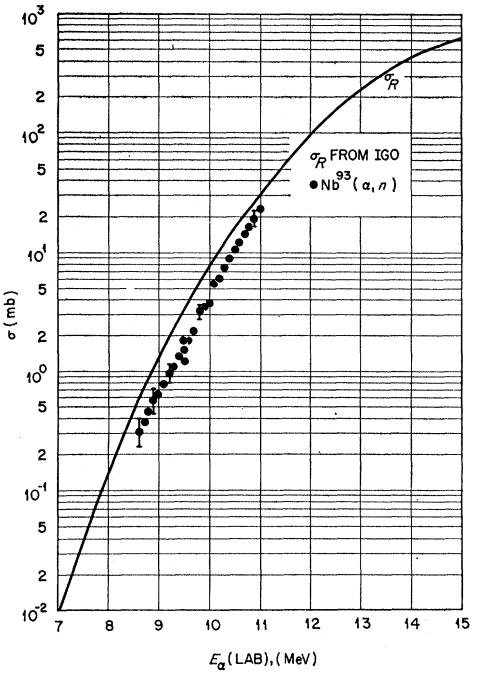

FIG. 9. The (α,n) cross section for Nb^{93} is shown together with Igo's predicted total reaction cross section.

sum of the $(\alpha,p)+(\alpha,\alpha')$ cross sections must be several times larger than the (α,n) cross section. The cross section has an irregular shape above $E_\alpha=9$ MeV. The

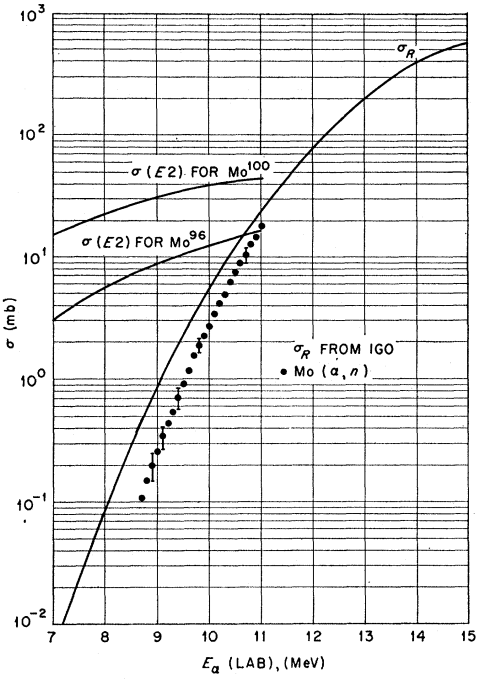

FIG. 10. The (α,n) cross section for normal molybdenum is shown together with Igo's predicted total reaction cross section. The Coulomb excitation cross sections for the excitation of the first 2+ states of Mo^{100} and Mo^{96} are also shown.

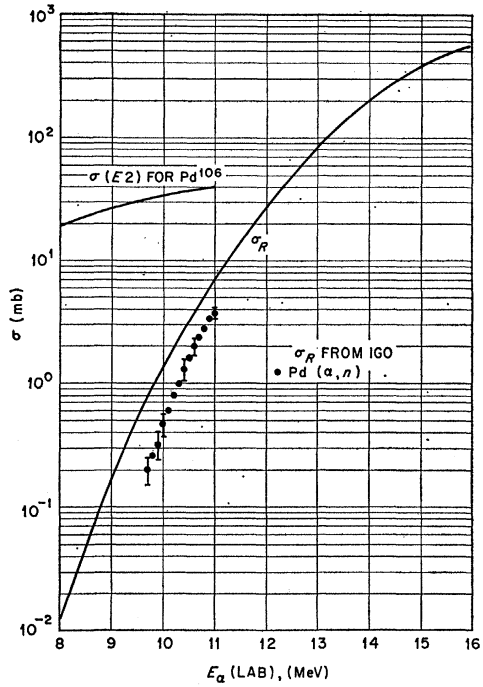

FIG. 11. The (α,n) cross section for normal palladium is shown together with Igo's predicted total reaction cross section. The Coulomb excitation cross section for the excitation of the first 2+ state of Pd^{106} is also shown.

(α,pn) reaction has a threshold at the indicated energy (E_α=9.45 MeV). This reaction competes with the (α,p) reaction and thus serves as an additional source of neutrons. However, the threshold for the (α,pn) reactions is somewhat high to account for the observed irregular shape.

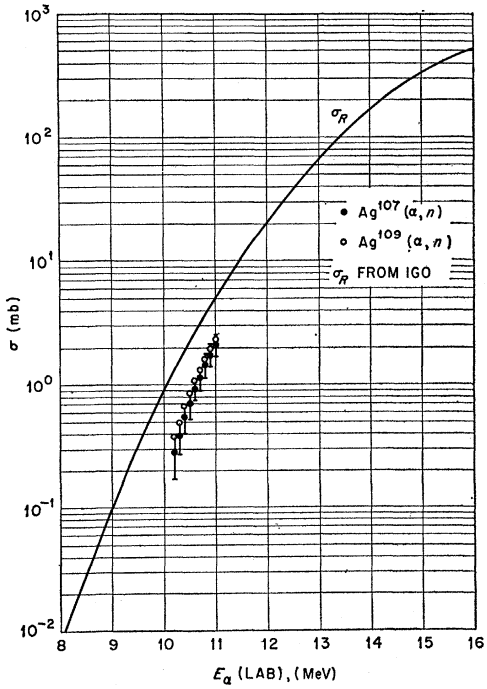

FIG. 12. The (α,n) cross sections for Ag^{107} and Ag^{109} targets are shown together with Igo's predicted total reaction cross section.

Figures 8 to 13 show (α,n) cross sections obtained for the heavier elements zirconium, niobium, molybdenum, palladium, silver, and indium. With increasing Z the cross sections become progressively smaller and this restricted the meaningful measurements to a small region at the higher bombarding energies. Igo's predicted values for the total reaction cross section are also shown. In all cases the (α,n) cross sections are somewhat smaller than the predicted total reaction cross section and they are therefore consistent with them.

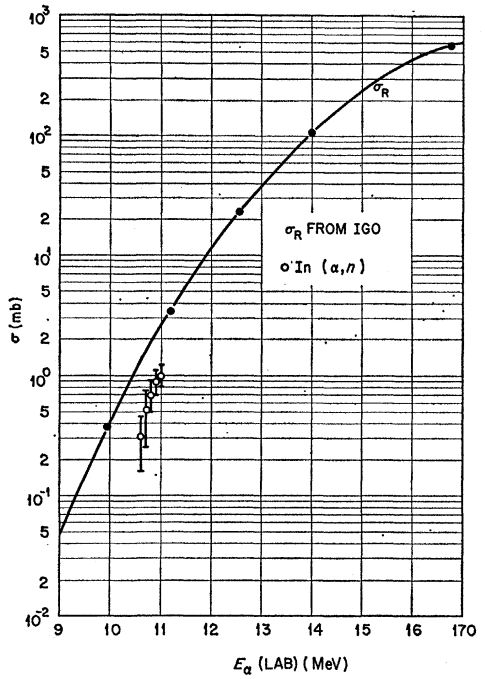

FIG. 13. The (α,n) cross section for indium is shown together with the total reaction cross section predicted by Igo.

A few representative Coulomb excitation cross sections for excitation of the first 2+ state are shown in Figs. 8, 10, and 11 for zirconium, molybdenum, and palladium, respectively. The comparison of these cross sections with the optical-model reaction cross section shows how much more slowly the Coulomb excitation cross sections vary with α-particle energy. As is expected, at lower α-particle energies the Coulomb excitation cross sections are several orders of magnitude larger than the predicted reaction cross section. On the other hand, the curves suggest that at high energies the Coulomb excitation cross section is quite small compared to the total reaction cross section.

The influence of Coulomb excitation, which is also a type of direct interaction, could be explicitly included

TABLE III. Summary of observed (α,n) thresholds. The observed (α,n) neutron thresholds are listed in column 2 for the reaction given in column 1. Column 3 lists the Q values obtained from the thresholds. For comparison, the Q values given in the Nuclear Data Tables are listed in column 4.

Reaction	E_{Th}(MeV)	Q(MeV) Exptl	Q(MeV) Mass tables
$Cu^{63}(\alpha,n)Ga^{66}$	8.16±0.03	−7.67±0.03	−7.513±0.032
$Cu^{65}(\alpha,n)Ga^{68}$	6.16±0.04	−5.80±0.04	−5.843±0.12
$Ni^{58}(\alpha,n)Zn^{61}$	10.49±0.03	−9.81±0.03	−9.680±0.300
$Ni^{60}(\alpha,n)Zn^{63}$	8.50±0.04	−7.97±0.04	−7.905±0.007
$Ni^{62}(\alpha,n)Zn^{65}$	6.93±0.04	−6.51±0.04	−6.474±0.006
$Zn^{64}(\alpha,n)Ge^{67}$	9.82±0.06	−9.24±0.06	−9.190±0.100
$Zn^{66}(\alpha,n)Ge^{69}$	7.98±0.03	−7.52±0.03	−7.542±0.030
$Zn^{68}(\alpha,n)Ge^{71}$	5.96±0.04	−5.63±0.04	−5.858±0.048

in the optical-model analyses by adding, for example, a relatively long-range term in the potential of the type r^{-3} to take into account $E2$ Coulomb excitation. The inclusion of Coulomb excitation in the optical-model analysis at intermediate energies (near the top of the barrier) has recently been considered by Bassel *et al.*[8]

The highly enriched isotopic targets of copper, nickel, and zinc allowed the observation of rather sharp thresholds for the onset of the (α,n) reaction. Eight of these thresholds are shown in Figs. 14 and 15. It was

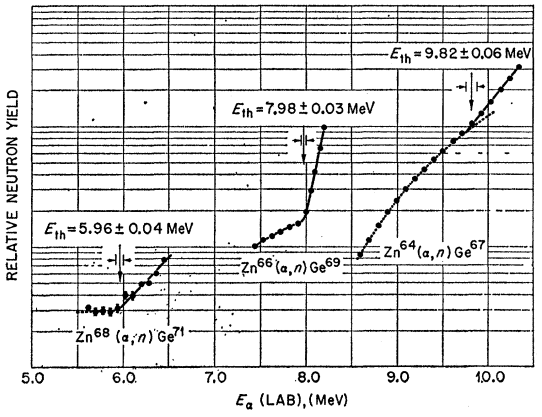

FIG. 14. Observed (α,n) thresholds for targets of Zn^{68}, Zn^{66}, and Zn^{64}.

[8] R. H. Bassel, G. R. Satchler, R. M. Drisko, and E. Rost, Phys. Rev. **128**, 2693 (1962).

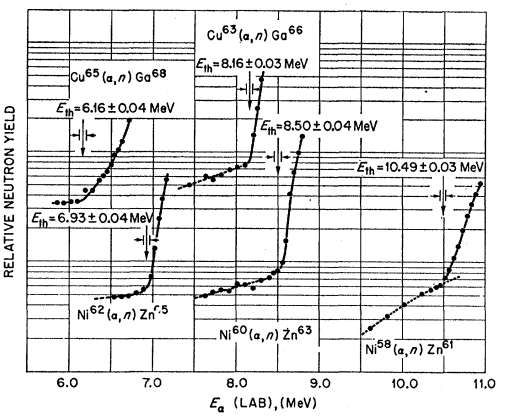

FIG. 15. Observed (α,n) thresholds for targets of Cu^{65}, Cu^{63}, Ni^{62}, Ni^{60}, and Ni^{58}.

especially important to have targets of high enrichment for those nuclei with high thresholds to reduce the large thick target neutron yield from the other isotopes with lower (α,n) thresholds.

The thresholds were determined to an accuracy of approximately ±40 keV. The observed values with the assigned errors are listed in column 2 of Table III. Column 3 of Table III lists the corresponding Q values listed in the *1960 Nuclear Data Tables*.[9]

The agreement between the two sets of Q values is quite good for the three target nuclei Cu^{65}, Ni^{62}, and Zu^{66}. The Q values for target nuclei Ni^{58} and Zn^{64} are also consistent but the errors on the values listed in the *Nuclear Data Tables* are quite large for these two nuclei. The present results can be regarded as giving more accurate information on the masses of Zn^{61} and Ge^{67} than has previously been available. The Q values for Cu^{63} and Zn^{68} targets are in poor agreement with those listed in the *Nuclear Data Tables*. For Cu^{63}, the difference in Q values is 160 keV whereas the quoted errors are both ±30 keV. Similarly, the difference for Zn^{68} is 230 keV whereas the errors are ±40 and ±48 keV.

[9] *1960 Nuclear Data Tables* (Printing and Publishing Office, National Academy of Sciences–National Research Council, Washington, D. C., 1960), Part 1, F. Everling, L. A. Koenig, J. H. E. Mattauch, and A. H. Wapstra; Part 2, L. A. Koenig, J. H. E. Mattauch, and A. H. Wapstra.